

HIGH-RESOLUTION HYDRODYNAMIC SIMULATION OF TIDAL DETONATION OF A HELIUM WHITE DWARF BY AN INTERMEDIATE MASS BLACK HOLE

ATARU TANIKAWA^{1,2}

¹Department of Earth Science and Astronomy, College of Arts and Sciences, The University of Tokyo, 3-8-1 Komaba, Meguro-ku, Tokyo 153-8902, Japan; tanikawa@ea.c.u-tokyo.ac.jp

²RIKEN Advanced Institute for Computational Science, 7-1-26 Minatojima-minami-machi, Chuo-ku, Kobe, Hyogo 650-0047, Japan

ABSTRACT

We demonstrate tidal detonation during a tidal disruption event (TDE) of a helium (He) white dwarf (WD) with $0.45M_{\odot}$ by an intermediate mass black hole (IMBH) by extremely high-resolution simulations. Tanikawa et al. (2017) have showed tidal detonation in previous studies results from unphysical heating due to low-resolution simulations, and such unphysical heating occurs in 3-dimensional (3D) smoothed particle hydrodynamics (SPH) simulations even with 10 million SPH particles. In order to avoid such unphysical heating, we perform 3D SPH simulations up to 300 million SPH particles, and 1D mesh simulations using flow structure in the 3D SPH simulations for 1D initial conditions. The 1D mesh simulations have higher resolution than the 3D SPH simulations. We show tidal detonation occurs, and confirm this result is perfectly converged with different space resolution in both 3D SPH and 1D mesh simulations. We find detonation waves independently arises in leading parts of the WD, and yield large amounts of ^{56}Ni . Although detonation waves are not generated in trailing parts of the WD, the trailing parts would receive detonation waves generated in the leading parts, and would leave large amounts of Si group elements. Eventually, this He WD TDE would synthesize ^{56}Ni of $0.30M_{\odot}$ and Si group elements of $0.08M_{\odot}$, and could be observed as a luminous thermonuclear transient comparable to type Ia supernovae.

Keywords: black hole physics — hydrodynamics — nuclear reactions, nucleosynthesis, abundances — supernovae: general — white dwarfs

1. INTRODUCTION

A tidal disruption event (TDE) is a phenomenon in which a star is tidally disrupted by a black hole (BH). TDEs have luminosities powered by accretion of stellar debris onto a BH. So far, many TDEs have been found (see reviews by Komossa 2015; Achettil et al. 2017; Stone et al. 2018). In most of these TDEs, main sequence (MS) stars are disrupted by massive black holes (MBH) with 10^6M_{\odot} to 10^8M_{\odot} . These TDEs can be useful for measuring physical quantities of MBHs, such as mass and spin.

Studies of MS TDEs are aimed at MBHs, whereas TDEs of white dwarfs (WDs) can contribute to studies of intermediate mass black holes (IMBHs). Similarly to MS TDEs by IMBHs, WD TDEs by IMBHs have bright flares driven by accretion of their debris onto the IMBHs (Zalamea et al. 2010; Clausen & Eracleous 2011; Haas et al. 2012; Cheng & Bogdanović 2014; MacLeod et al. 2014; Shiokawa et al. 2015; Ioka et al. 2016; Law-Smith et al. 2017). Moreover, luminosities of WD TDEs could be powered by radioactive decay of nuclei synthesized by tidal detonation (e.g.

Luminet & Pichon 1989). The tidal detonation could occur as follows. During a TDE, a WD is elongated in the direction of the orbital plane (hereafter, x - y plane), and however is compressed in the direction perpendicular to the x - y plane (hereafter, z -direction). The compression heats the WD, and triggers explosive nuclear reactions. Finally, the explosive nuclear reactions synthesize large amounts of radioactive nuclei (Rosswog et al. 2008, 2009). MacLeod et al. (2016) have showed the luminosity of the synthesized radioactive nuclei at peak is larger than the accretion-powered luminosity (the Eddington luminosity of an IMBH) by two orders of magnitude. WD TDEs can launch jets whose luminosities are much larger than the radioactive luminosity if observers are along with the jet axis (van Velzen et al. 2011, 2013; Krolik & Piran 2011, 2012; Tchekhovskoy et al. 2014; MacLeod et al. 2014), although the jet luminosities strongly depends on line-of-sight directions. WD TDEs also emit gravitational wave (GW) radiation, although the GW frequency is fit to space-based GW detectors (East 2014). Current and future optical surveys can find many IMBHs, searching for tidal detonation of WDs.

The abundance of IMBHs will be an important key to reveal the formation process of MBHs.

Tanikawa et al. (2017), hereafter Paper I, have revisited tidal detonation of a WD. Paper I has shown adiabatic compression cannot heat a WD sufficiently for tidal detonation in the following reason. A WD should be adiabatically compressed by at least 4 orders of magnitude in order to experience tidal detonation. However, such adiabatic compression is impossible. A WD can approach an IMBH without swallowing nor swallowed by the IMBH when a penetration factor β is less than 20 (Luminet & Pichon 1989; Rosswog et al. 2009; Kawana et al. 2017), where β is defined as the ratio of a tidal disruption radius to a pericenter distance. The size of a WD in the z -direction, z_{\min} , can be written as $z_{\min}/R_{\text{wd}} \sim \beta^{-3}$ at the pericenter (Stone et al. 2013), where R_{wd} is the original radius of the WD. Hence, a WD is compressed by at most a factor of 8000, and in reality is less compressed, since it is elongated in the direction of x - y plane. Luminet & Pichon (1989) have argued a helium (He) WD can experience tidal detonation by adiabatic compression. However, their He WD has unrealistically high density, $\sim 10^7 \text{ g cm}^{-3}$, or unrealistically high mass, $0.6M_{\odot}$. Note that the upper limit of He WD mass is about $0.5M_{\odot}$ (Parsons et al. 2017). If a He WD has such high density, tidal detonation can occur when the He WD is compressed only by two orders of magnitude. Wilson & Mathews (2004) have suggested compression of a WD causes the central density to exceed the threshold for pycnonuclear reactions. However, they have overestimated the compression, since they have not taken into account stretch of the WD by a tidal field.

Thus, tidal detonation requires shock compression. A shock wave can arise when β is sufficiently larger than unity (Kobayashi et al. 2004). In the case of $\beta < 12$, where most of WD TDEs occur, the mechanism of shock generation is as follows (Brassart & Luminet 2008). A WD approaches to an IMBH, and is compressed in the z -direction. At some time, the central pressure of the WD increases instantaneously. Then, the WD bounces back. The bounce generates a pressure wave propagating outward along the z -direction. The pressure wave steepens into a shock wave near the WD surface.

However, the generation of a shock wave is not sufficient condition for tidal detonation. The shock wave has to raise temperature so highly that nuclear reactions start. Moreover, the nuclear reactions have to be explosive. Otherwise, they cease soon.

In this paper, we investigate whether a shock wave arising during a WD TDE triggers tidal detonation. Rosswog et al. (2008, 2009) have reported tidal detonation occurs in He WDs and CO WDs by 3-dimensional (3D) smoothed particle hydrodynamics (SPH) simula-

tions. However, they have not shown shock generation in their simulations explicitly. Paper I have shown tidal detonation in Rosswogs' simulations is triggered by spurious heating due to failure to resolve the height of a WD from the x - y plane. Paper I have demonstrated high-resolution 1-dimensional (1D) mesh simulations in which shock compression generates tidal detonation. Here, initial conditions of the 1D mesh simulations are WD structure along with the z -direction which is extracted from our 3D SPH simulations. However, in Paper I, our method to make 1D initial conditions is not sophisticated. Density profiles in the 1D mesh simulations tend to be higher than in the 3D SPH simulations during the evolution. This is because 3D effects, such as a tidal field, are ignored in the 1D mesh simulations. Since nuclear reactions become active under higher density environment, shock compression is easier to trigger tidal detonation in the 1D mesh simulations than in reality. Therefore, Paper I have not confirmed whether tidal detonation occurs or not. Moreover, the overestimate of density affects nucleosynthesis if tidal detonation occurs.

For this purpose, we develop a method to make 1D initial conditions extracting WD structure along with the z -direction from 3D SPH simulations. Owing to this method, density evolution in 1D mesh simulations is the same as in 3D SPH simulations. Using this method and high-resolution simulations, we make it clear whether tidal detonation occurs during a WD TDE. To come to the point, tidal detonation occurs. Thus, we investigate its nucleosynthesis. It is the first time that numerical simulations demonstrate tidal detonation of a WD triggered by shock compression.

The paper is structured as follows. In section 2, we describe our method which we validate in Appendix A. In section 3, we show our simulation results. We discuss about nucleosynthesis of this WD TDE in section 4. Finally, we summarize our paper in section 5. In this paper, we adopt CGS units unless specified.

2. METHOD

We follow tidal detonation of WD TDEs as follows. We perform 3D SPH simulations to follow overall WD TDEs. In order to make initial conditions of 1D mesh simulations, we extract WD structure along with z -direction from the 3D SPH results. Finally, we perform 1D mesh simulations. In subsection 2.1, we present our method of 3D SPH simulations. In subsection 2.2, we show how to make 1D initial conditions. In subsection 2.3, we describe our method of 1D mesh simulations.

2.1. 3D SPH simulation

Our SPH method is similar to those in Tanikawa et al. (2017). We adopt the vanilla-ice SPH equations for

our SPH code. Our SPH kernel function is Wendland C^2 Kernel (Wendland 1995; Dehnen & Aly 2012). A given particle has neighbor particles of about 120. Our artificial viscosity is the same as proposed by Monaghan (1997), and dependent on the strength of a shock wave (Morris & Monaghan 1997). We suppress the viscosity from shear motion, using Balsara’s switch (Balsara 1995). We calculate gravitational forces among particles with adaptive gravitational softening (Price & Monaghan 2007). We parallelize our SPH code on distributed-memory systems using FDPS (Iwasawa et al. 2016), and speed up explicit AVX instructions (e.g. Tanikawa et al. 2012, 2013). We adopt the Helmholtz equation of state (EoS) without Coulomb corrections (Timmes & Swesty 2000). We do not couple our SPH code with nuclear reaction networks.

We choose an initial condition of a 3D SPH simulation as follows. Our WD model has $0.45M_{\odot}$ and pure He composition, which is nearly the upper limit of He WD mass (Parsons et al. 2017). It has no spin. The numbers of SPH particles for the WD (hereafter N_{sph}) are 4.7, 9.4, 19, 38, 75, 150, and 300 millions, hereafter called 4.7M, 9.4M, 19M, 38M, 75M, 150M, and 300M, respectively. We relax the configurations of SPH particles in the same way as Tanikawa et al. (2015). We approximate IMBH gravitational potential as Newton potential. The IMBH mass is $300M_{\odot}$. The orbit of the WD is parabolic around the IMBH. The penetration factor β is 7. The IMBH does not irrupt into nor swallow the WD. This is true even if we consider general relativity for the IMBH gravity, using a generalized Newtonian potential (Tejeda & Rosswog 2013). An IMBH with $300M_{\odot}$ permits the closest encounter of a WD without irrupting into and swallowing the WD among IMBHs (Kawana et al. 2017). The initial distance between the WD and IMBH is twice the tidal disruption radius. We use $t_{3\text{D}}$ as the time from the starting time of a 3D simulation. Then, the WD passes the pericenter during $t_{3\text{D}} = 6$ s to $t_{3\text{D}} = 7$ s after 3D simulations start in all the N_{sph} cases.

2.2. 1D initial conditions

We make 1D initial conditions, extracting density and velocity profiles in the z -direction from a WD whose evolution is followed by a 3D SPH simulation. Hereafter, we call a portion of WD structure extracted along the z -direction “ z -column”, and velocity in the z -direction “ z -velocity”. We should minimize difference of density and z -velocity evolution between 1D and 3D simulations. The difference comes from 3D effects, such as a tidal field. In order to minimize the 3D effects, we devise how to choose the time and place of z -columns of the WD. If we follow 1D evolution for a long term, the 3D effects become significant. Thus, we should fol-

low 1D evolution for as short a term as possible. For this purpose, we start a 1D mesh simulation just before tidal detonation is likely to occur. The tidal detonation is triggered by a shock wave. The shock wave is formed from steepening of a pressure wave generated by bounce of WD materials on the x - y plane. In order for the pressure wave to steepen into the shock wave, relative velocity between WD materials on x - y plane and on the WD surface is supersonic (Brassart & Luminet 2008). Thus, we extract z -columns in which WD materials on the surface approach the x - y plane at speed of Mach 4 before the bounce. Moreover, we select the densest z -columns among the above z -columns, since such z -columns are easy to be detonated. In Appendix A.1, we show our method minimizes 3D effects.

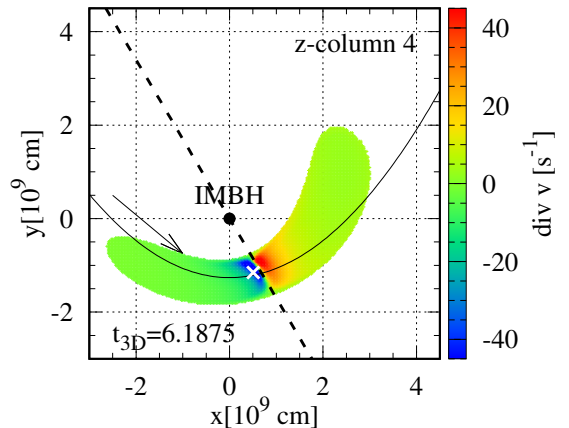


Figure 1. Divergence of velocity on the x - y plane at the indicated time in 3D SPH simulation for the $N_{\text{sph}} = 38\text{M}$ case. The IMBH is located at the coordinate origin. The solid curves show the orbit of the WD on the assumption that the WD is a point mass, and the arrows indicate the direction of the WD orbit. The dashed line in each panel ($y = -1.7x$) is a boundary dividing the WD into shrinking and expanding parts. White crosses indicate z -column 4, whose density is the highest among extracted z -columns.

We apply the above method to the $N_{\text{sph}} = 38\text{M}$ case. For the other N_{sph} cases, we extract z -columns whose time and place are the same as those in the $N_{\text{sph}} = 38\text{M}$ case, in order to perform a convergence check with different N_{sph} of 3D SPH simulations (see Appendix A.5). We extract 9 z -columns from 3D SPH simulation for each N_{sph} case. We refer to these z -columns as z -columns 1, 2, ..., and 9 in order from the front in the orbital direction of the WD. As an example, we show z -column 4 extracted from the $N_{\text{sph}} = 38\text{M}$ case in Figure 1. The z -column has the highest density among extracted z -columns. The z -column is located in a shrinking region close to boundaries between shrinking and expanding regions. Therefore, the z -column is located just before bounce.

Figure 2 shows the positions extracted z -columns at

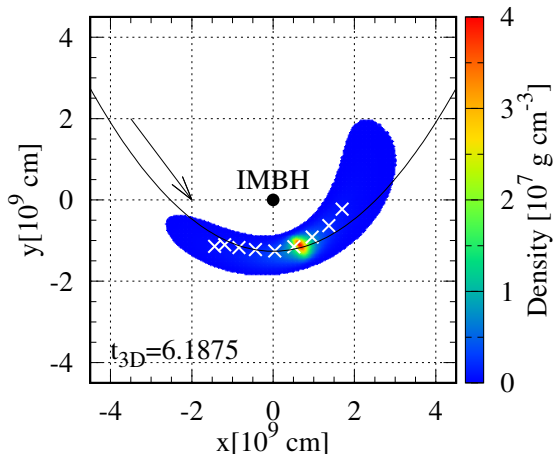


Figure 2. Density on the x - y plane at $t_{3D} = 6.1875$ s in 3D SPH simulation for the $N_{\text{sph}} = 38M$ case. The IMBH is located at the coordinate origin. White crosses indicate z -columns 1 - 9 at $t_{3D} = 6.1875$ s from right to left.

$t_{3D} = 6.1875$ s. From right to left, z -columns 1 - 9 are indicated by white crosses. Note that we do extract z -column 4 at this time, however we do not extract the other z -columns at this time. We extract z -column x at $t_{3D} = 6 + (x - 1)/16$ s. These z -columns are located in a shrinking region close to boundaries between shrinking and expanding regions, similarly to z -column 4. Since z -column 4 is closest to the maximum density point of the WD among these z -columns, z -columns 1 - 3 precede the maximum density point, and z -columns 5 - 9 follow the maximum density point. Materials preceding z -column 1 have $0.05M_{\odot}$, and materials following z -column 9 have $0.01M_{\odot}$. This means that these z -columns cover about 90 % of the WD.

In order to make 1D initial conditions, we calculate density and z -velocity of the z -columns, using SPH kernel interpolation. We do not use temperature of 3D SPH simulations, and set temperature to be 10^6 K. Although we set temperature to 10^5 K, 10^6 K, and 10^7 K, the temperature does not affect results of 1D mesh simulations.

For the $N_{\text{sph}} = 300M$ case, we indicate the calculated density and z -velocity by solid curves in Figure 3. As reference, we also plot density and z -velocity of SPH particles in z -column 4. The density and z -velocity profiles for the 1D initial condition are in a good agreement with those in the 3D SPH simulation, except the edge of the z -column. In Appendix A.3, we describe the discrepancy at the edge does not affect the emergence of tidal detonation.

2.3. 1D mesh simulation

We use the FLASH code (Fryxell et al. 2000) for 1D mesh simulations. The FLASH code is an Eulerian code. We use uniform mesh, switching off adaptive mesh refinement. We adopt the piecewise parabolic method

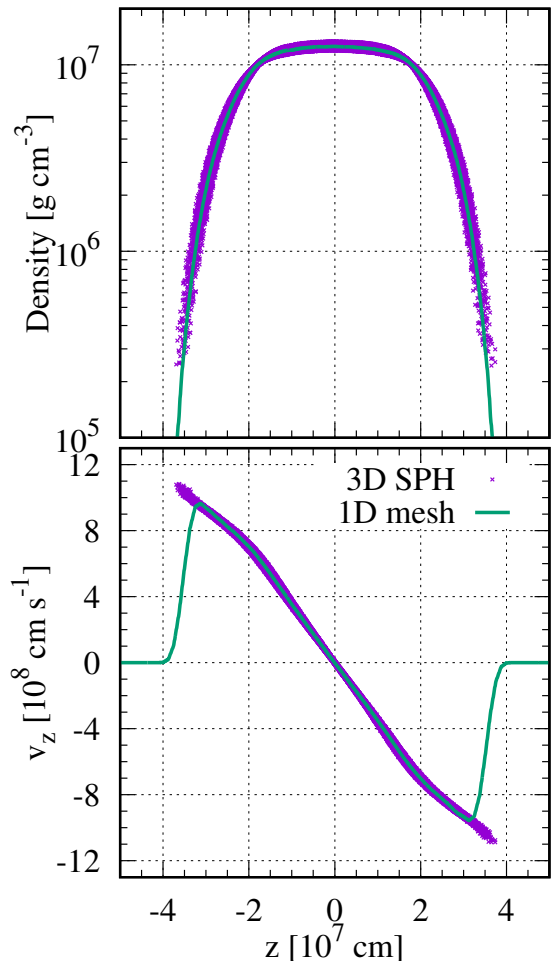


Figure 3. Profiles of density and z -velocity in z -column 4 in 3D SPH simulation for the $N_{\text{sph}} = 300M$ case. Solid curves show 1D profiles used for 1D initial conditions. Crosses indicate density and z -velocity of SPH particles in the 3D SPH simulation.

(Colella & Woodward 1984) for the gas hydrodynamic solver. Our EoS and nuclear reaction networks are the Helmholtz EoS and Aprox13, respectively. Our timestep criterion is the minimum value of the hydrodynamics timestep and nuclear reaction timestep. The hydrodynamic timestep is 10 % of the Courant-Friedrichs-Lewy number and the nuclear reaction timestep is 1 % of the ratio of the specific internal energy to the specific nuclear energy-generation rate. We do not consider self gravity of fluids. In most of 1D mesh simulations, we do not include the IMBH gravity, however we partly include the IMBH gravity in order to investigate its effect (see Appendix A.2).

We set up calculation domain as follows. The domain geometry is Cartesian. We have four cases of the domain range: $0 \leq z/10^8 \text{cm} \leq 0.50$, $|z/10^8 \text{cm}| \leq 0.5$, $|z/10^8 \text{cm}| \leq 1.0$, and $|z/10^8 \text{cm}| \leq 2.0$. The number of meshes is 6400 in all the cases. Therefore, the mesh sizes are 0.78×10^4 cm, 1.56×10^4 cm, 3.13×10^4 cm,

and 6.25×10^4 cm. We adopt the domain range of $|z/10^8 \text{cm}| \leq 4.0$ unless specified, and adopt the other ranges for resolution study (see Appendix A.4). The domain fully covers 1D WD structure in the cases of the domain ranges of $|z/10^8 \text{cm}| \leq 1.0$, $|z/10^8 \text{cm}| \leq 2.0$, and $|z/10^8 \text{cm}| \leq 4.0$. In these cases, the boundary condition is the outflow boundary at both the edges of the domain. In the case of the domain range of $0 \leq z/10^8 \text{cm} \leq 0.50$, the domain covers only half the 1D WD structure with $z \geq 0$. Thus, the boundary condition at $z = 0$ is the reflection boundary, and the boundary condition at the other edge is the outflow boundary.

We use t_{1D} as the time from the starting time of a 1D mesh simulation. The relation between t_{1D} and t_{3D} is $t_{1D} = t_{3D} - (6 + (x - 1)/16)$ s for z -column x .

We use initial conditions extracted from 3D SPH simulation with $N_{\text{sph}} = 300\text{M}$ unless specified.

3. RESULTS

We show success and failure cases of tidal detonation in order to identify the emergence of tidal detonation easily. First, we present a failure case. The right four panels of Figure 4 show the time evolution of profiles of density, z -velocity, temperature, and nuclear compositions of z -column 8. At the beginning, the WD materials shrink in the z -direction. At $t_{1D} \sim 0.0234$ s, these materials bounce back, and a pressure wave is generated. At $t_{1D} \sim 0.0313$ s, the pressure wave steepens into a shock wave. The shock wave is located at $z \sim 1.5 \times 10^7$ cm at $t_{1D} \sim 0.0391$ s, and indicated by vertical dotted blue lines. The shock wave raises temperature of a part of the materials. The temperature rise ignites nuclear reactions. However, this nuclear reactions burn only small amounts of ^4He , and cease soon.

In this case, tidal detonation fails. This is because the shock wave heats too a small region to trigger a detonation wave. The region heated by the shock wave has $\sim 2 \times 10^6$ g cm $^{-3}$. According to Holcomb et al. (2013), detonation in pure He composition arises only from a hotspot with size of $> 10^6$ cm if the density is $\sim 2 \times 10^6$ g cm $^{-3}$. However, the size of the heated region is much smaller than 10^6 cm.

Next, we introduce a success case of tidal detonation. The left four panels of Figure 4 show the time evolution of z -column 7. The first-half evolution is similar to that of z -column 8. At the initial time, the WD materials shrink. They bounce back at $t_{1D} \sim 0.0234$ s, and a pressure wave is generated. At $t_{1D} \sim 0.0313$ s, the pressure wave steepens into a shock wave. The shock wave raises temperature of a part of the materials. After that, the evolution is different from that of z -column 8. The temperature rise triggers explosive nuclear reactions. Since the nuclear reactions rapidly expand the materials, they generate both forward and reverse shock waves. The for-

ward and reverse shock waves can be respectively seen at $z \sim 1.75 \times 10^7$ cm (vertical dotted blue lines) and 0.50×10^7 cm at $t_{1D} = 0.0391$ s (vertical dotted red lines) in the z -velocity panel of Figure 4 for z -column 7. The reverse shock wave accompanies a detonation wave. In fact, behind the reverse shock wave, large amounts of ^4He and ^{56}Ni are depleted and yielded, respectively. Note that the reverse shock wave moves leftward in Figure 4.

In this case, tidal detonation succeeds. This is because the shock wave heats a region large enough to trigger a detonation wave. The region heated by the shock wave has $\sim 5 \times 10^6$ g cm $^{-3}$. According to Holcomb et al. (2013), detonation in pure He composition arises only from a hotspot with size of $> 10^5$ cm if the density is $\sim 5 \times 10^6$ g cm $^{-3}$. The size of the heated region is much larger than 10^5 cm.

The evidence of tidal detonation is the presence of a reverse shock wave. A reverse shock wave can be easily seen in a z -velocity profile.

Figure 5 shows the z -velocity profiles for z -columns 1 - 9 just after pressure waves steepens into shock waves. We can see reverse shock waves of z -columns 1 - 7 indicated by arrows. In other words, tidal detonation occurs in z -columns 1 - 7, and does not in z -columns 8 - 9. The difference between the former and latter z -columns is the distances from the IMBH. As seen in Figure 2, the leading part of the WD tends to pass more closely to the IMBH than the trailing part. Therefore, the former z -columns are closer to the IMBH (more compressed) than the latter z -columns. We expect the materials preceding z -column 1 succeed in tidal detonation, and the materials following z -column 9 fail in tidal detonation.

Figure 6 shows the profiles of nuclear elements tidal detonation yields in z -columns 1, 4, and 7. The nuclear reactions have been already finished in z -column 7 at $t_{1D} = 0.625$ s. Most of materials have been burned by this time. It seems that large amounts of unburned materials are left at $z > 0.7 \times 10^8$ cm. However, mass at $z > 0.7 \times 10^8$ cm is much smaller than the total mass, since density at $z > 0.7 \times 10^8$ cm is much smaller than at $z < 0.7 \times 10^8$ cm. The nuclear reactions synthesize 80 % of ^{56}Ni , and leave 20 % of ^4He in mass. There are small amounts of Si group elements (^{28}Si , ^{32}S , ^{36}Ar , ^{40}Ca , and ^{44}Ti), and their mass fraction is 0.3 %. The reason for the small amounts of Si group elements is that detonated materials have high density ($\gtrsim 10^7$ g cm $^{-3}$). Note that Si group elements are synthesized when a detonation wave proceeds in a region with density of $\lesssim 10^6$ g cm $^{-3}$.

In the cases of z -columns 1 and 4, we have not finished nuclear reactions. These 1D mesh simulations are largely time-consuming. Timestep becomes too small just before the detonation wave reaches the orbital plane ($z = 0$) due to nuclear reactions. Here, we make a con-

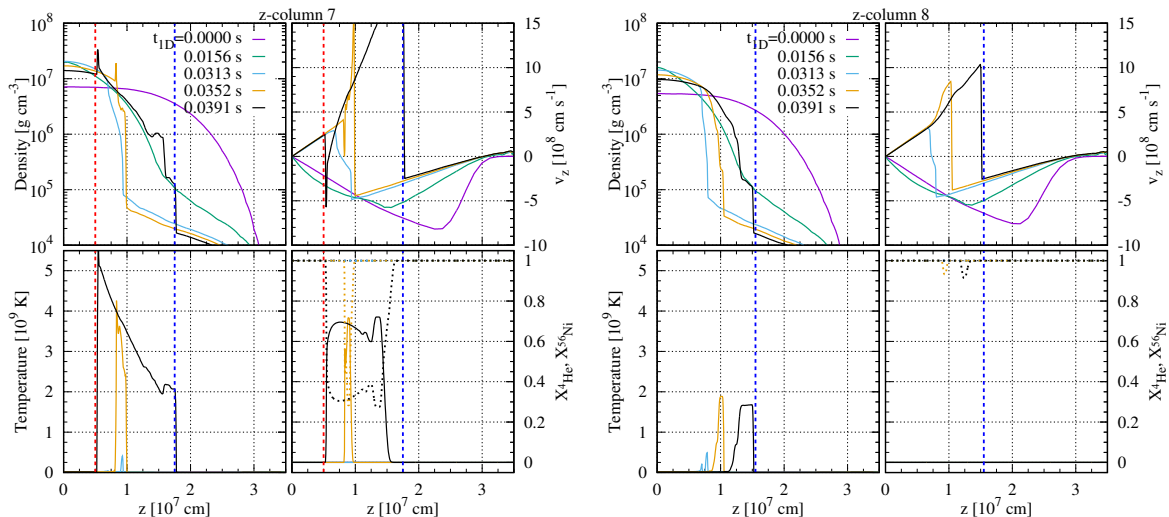


Figure 4. Time evolution of density, z -velocity, temperature, and nuclear composition profiles in z -column 7 (left four panels) and 8 (right four panels). The mass fractions of ${}^4\text{He}$ and ${}^{56}\text{Ni}$ are indicated by dotted and solid curves, respectively. Vertical dotted blue lines indicate forward shock waves, and vertical dotted red lines indicate a reverse shock wave accompanying a detonation wave.

jecture about nucleosynthesis in z -columns 1 and 4 from the results of z -column 7. In the second right panel of Figure 6, we show nuclear components in z -column 7 just before a detonation wave reaches the orbital plane. The nuclear components in z -columns 1, 4, and 7 are similar just before the detonation waves reach the orbital plane. Therefore, we expect nuclear components in these z -columns will be similar when nuclear reactions have finished.

The 1D mesh simulation in the case of z -column 7 has been finished in the following reason. Since z -column 7 follows z -columns 1 and 4, the former is less compressed than the latter. The former density at $z = 0$ is smaller. The nuclear reactions in z -column 7 are less active than in z -columns 1 and 4. Therefore, timestep in the case of z -column 7 does not become as small as in the case of z -columns 1 and 4.

4. DISCUSSION

We estimate overall nucleosynthesis in our WD TDE model. We also examine 3D effects for the nucleosynthesis.

We consider whether a detonation wave proceeds in the direction of the x - y plane. Figure 7 shows the position of z -column 7 (the white cross) and four arrows from z -column 7. These arrows point to four directions on the x - y plane. Hereafter, we refer to the direction of arrow X as the X-direction. The detonation wave from z -column 7 would not proceed in the A-, C-, and D-directions. The z -columns in the D-direction have been already detonated. The z -columns in the A- and C-directions are detonated simultaneously with z -column 7.

The detonation wave from z -column 7 would proceed

in the B-direction, if no detonation wave is generated from z -columns in the B-direction. If detonation waves are generated from z -columns in the B-direction, the detonation wave from z -column 7 would not proceed in the B-direction. Detonation waves from z -columns in the B-direction would be spontaneously generated before the detonation wave from z -column 7 reaches these z -columns. This is because the speed of the detonation wave ($\sim 10^9$ cm s $^{-1}$) is much slower than the orbital velocity of the WD ($\sim 8 \times 10^9$ cm s $^{-1}$).

Based on the above consideration, we can divide z -columns of a WD into two types. The first type is z -columns in which tidal detonation arises, such as z -columns 1 - 7. The second type is z -columns which tidal detonation arising in other z -columns reaches. Since tidal detonation succeeds in z -columns 7, and fails in z -columns 8, we assume that z -columns preceding z -column 7 are the first type, and that z -columns following z -column 7 are the second type. Note that leading parts are easier to be detonated than trailing parts, as described in section 3.

We discuss about the first type of z -columns. All these z -columns would be detonated independently of each other. These z -columns have mass of $0.37M_{\odot}$. Their nuclear compositions would be similar to those of z -columns 1, 4 and 7 (see Figure 6). Then, their nuclear compositions would be ${}^{56}\text{Ni}$ of $0.30M_{\odot}$ and ${}^4\text{He}$ of $0.07M_{\odot}$. There would be small amounts of Si group elements, $\sim 0.001M_{\odot}$.

We examine the second type of z -columns. They would be detonated by the detonation wave generated in z -column 7. From our simulation results, we find the detonation wave traverses these z -columns when these z -columns have density of $\sim 10^5$ g cm $^{-3}$. There-

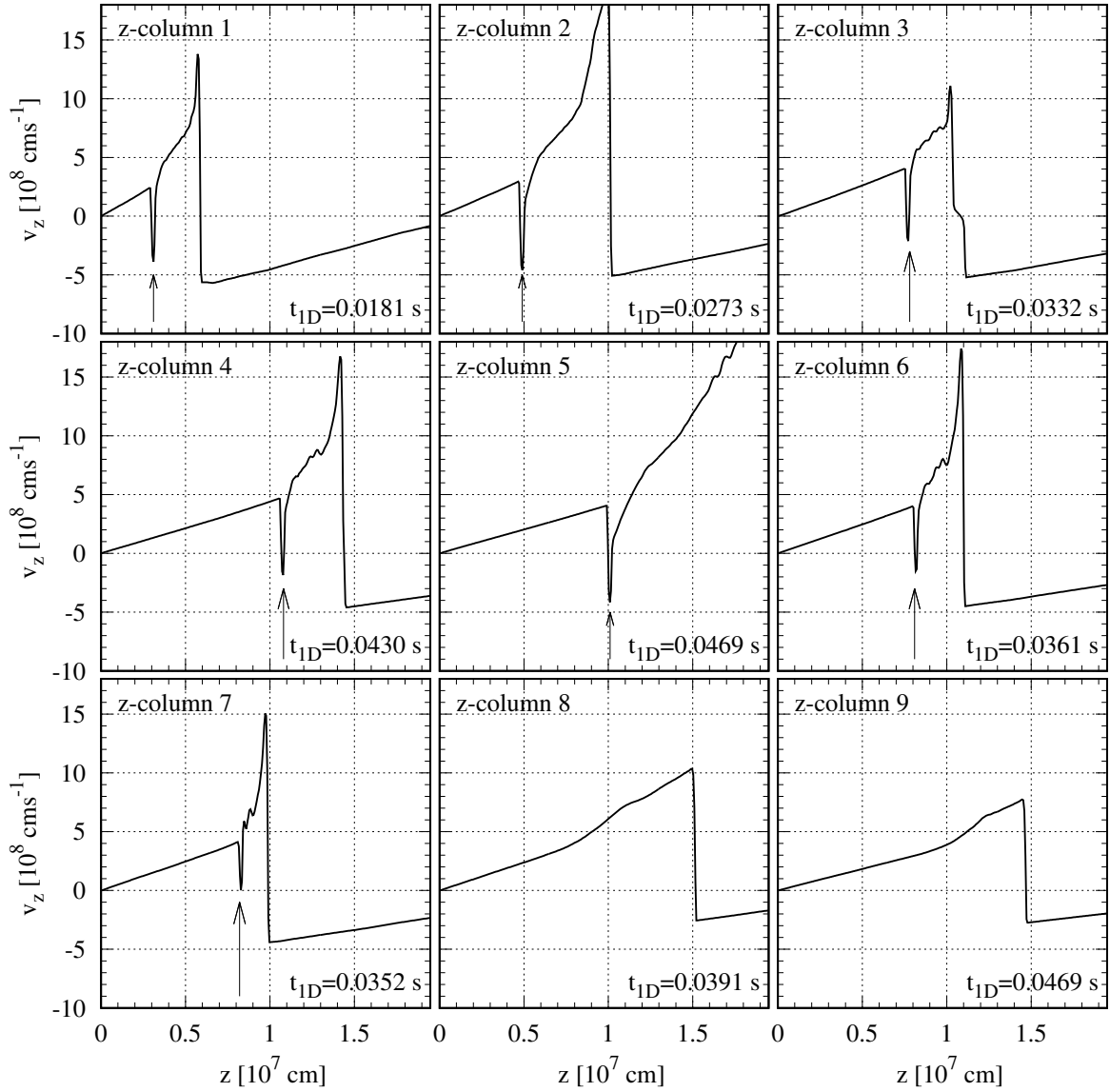


Figure 5. Profiles of z -velocity in z -columns 1 - 9 just after pressure waves steepen into shock waves. Arrows indicate reverse shock waves accompanying detonation waves.

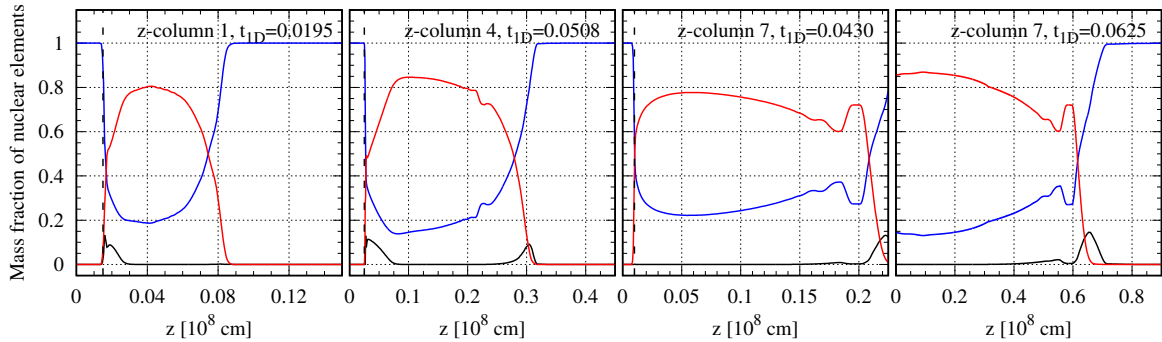


Figure 6. Profiles of nuclear elements in z -columns 1, 4 and 7. Blue, black, and red curves indicate mass fractions of ${}^4\text{He}$, Si group elements (${}^{28}\text{Si}$, ${}^{32}\text{S}$, ${}^{36}\text{Ar}$, ${}^{40}\text{Ca}$, and ${}^{44}\text{Ti}$), and ${}^{56}\text{Ni}$, respectively. Dashed lines indicate the positions of detonation waves. There is no dashed line in the right panel, since a detonation wave has reached the orbital plane ($z = 0$), and nuclear reactions have been already finished.

fore, the detonation wave would yield large amounts of

Si group elements in these z -columns (Holcomb et al.

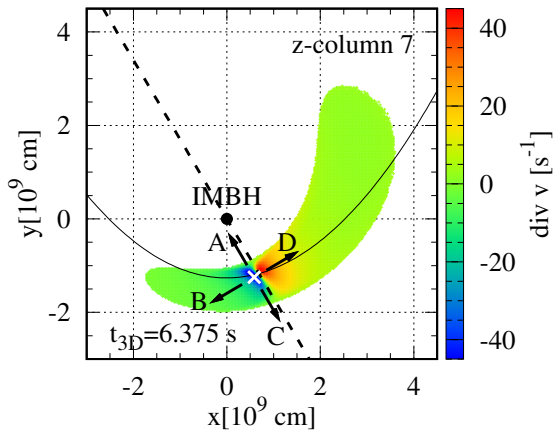


Figure 7. Divergence of velocity on the x - y plane at the indicated time in 3D SPH simulation for the $N_{\text{sph}} = 38 M$ case. The white cross indicates z -column 7. Four arrows from z -column 7 are depicted. Arrow A points to the direction of the IMBH. Arrow D points to the traveling direction of the WD. Arrows C and B point to the inverse directions of arrows A and D, respectively.

2013). Since these z -columns have $0.08M_{\odot}$, Si group elements of $0.08M_{\odot}$ would be synthesized.

In summary, our WD TDE model would yield ^{56}Ni of $0.30M_{\odot}$ and Si group elements of $0.08M_{\odot}$, and leave ^4He of $0.07M_{\odot}$. Since parts of them would be swallowed by the IMBH, all of them would not contribute to the luminosity of our WD TDE model. However, we do not investigate the subsequent evolution of the WD TDE. We cannot follow the orbit of the WD debris accurately, since we simplify the IMBH gravity as Newton gravity.

5. SUMMARY

We assess whether tidal detonation occurs true in WD TDEs. We choose a He WD with $0.45M_{\odot}$. We need prohibitively large calculation cost to follow tidal detonation of a WD TDE by 3D SPH simulations. Thus, we combine 1D mesh simulations with 3D SPH simulations. For 1D mesh simulations, we develop a method to extract 1D initial conditions from 3D SPH simulation data. Owing to the method, we can follow 1D evolution, not annoyed by 3D effects, such as a tidal field.

We show tidal detonation arises by shock heating. We emphasize it is the first time that numerical simulations demonstrate tidal detonation of a WD triggered

by shock heating. For this purpose, we perform severe convergence checks with different N_{sph} of 3D SPH simulations and with different space resolution of 1D mesh simulations. Tidal detonation succeeds in z -columns preceding z -column 7, and fails in z -columns following z -column 7. Leading parts are easier to be detonated in the following reason. Leading parts are more compressed by the IMBH than trailing parts, and tend to have higher density. A detonation wave is easier to occur in a higher density region, since nuclear reactions proceed more rapidly.

For z -columns preceding z -column 7, the detonation waves would yield large amounts of ^{56}Ni , since these z -columns have high density, $\sim 10^7 \text{ g cm}^{-3}$. Materials in z -columns following z -column 7 would be detonated by the detonation wave arising from z -column 7. In these z -columns, large amounts of Si group elements would be synthesized, since these z -columns have density $\sim 10^5 \text{ g cm}^{-3}$ when these z -columns receive the detonation wave. Eventually, our WD TDE model would synthesize ^{56}Ni of $0.30M_{\odot}$ and Si group elements of $0.08M_{\odot}$, and would leave ^4He of $0.07M_{\odot}$. Therefore, the WD TDE could be observed as a luminous thermonuclear transient comparable to type Ia supernovae.

Numerical computations were carried out on Cray XC30 at Center for Computational Astrophysics, National Astronomical Observatory of Japan, on Cray XC40 at Yukawa Institute for Theoretical Physics, Kyoto University, and on Oakforest-PACS at Joint Center for Advanced High Performance Computing. The software used in this work was in part developed by the DOE NNSA-ASC OASCR Flash Center at the University of Chicago. This research has been supported in part by MEXT program for the Development and Improvement for the Next Generation Ultra High-Speed Computer System under its Subsidies for Operating the Specific Advanced Large Research Facilities, and by Grants-in-Aid for Scientific Research (16K17656, 17H06360) from the Japan Society for the Promotion of Science.

Software: FLASH (Fryxell et al. 2000, 2010)

APPENDIX

A. VALIDATION OF OUR METHOD

A.1. Comparison between 3D and 1D simulations

In Figure A1, we compare the time evolution of z -columns 1, 4, 7, and 8 in the 3D SPH simulation of $N_{\text{sph}} = 300M$ with the time evolution of these z -columns in the 1D mesh simulation. For this comparison, we turn off nuclear reaction networks in the 1D mesh simulation. We find a good agreement between the 3D SPH and 1D mesh simulation results. Therefore, 3D effects, such as a tidal field, are not significant during this time.

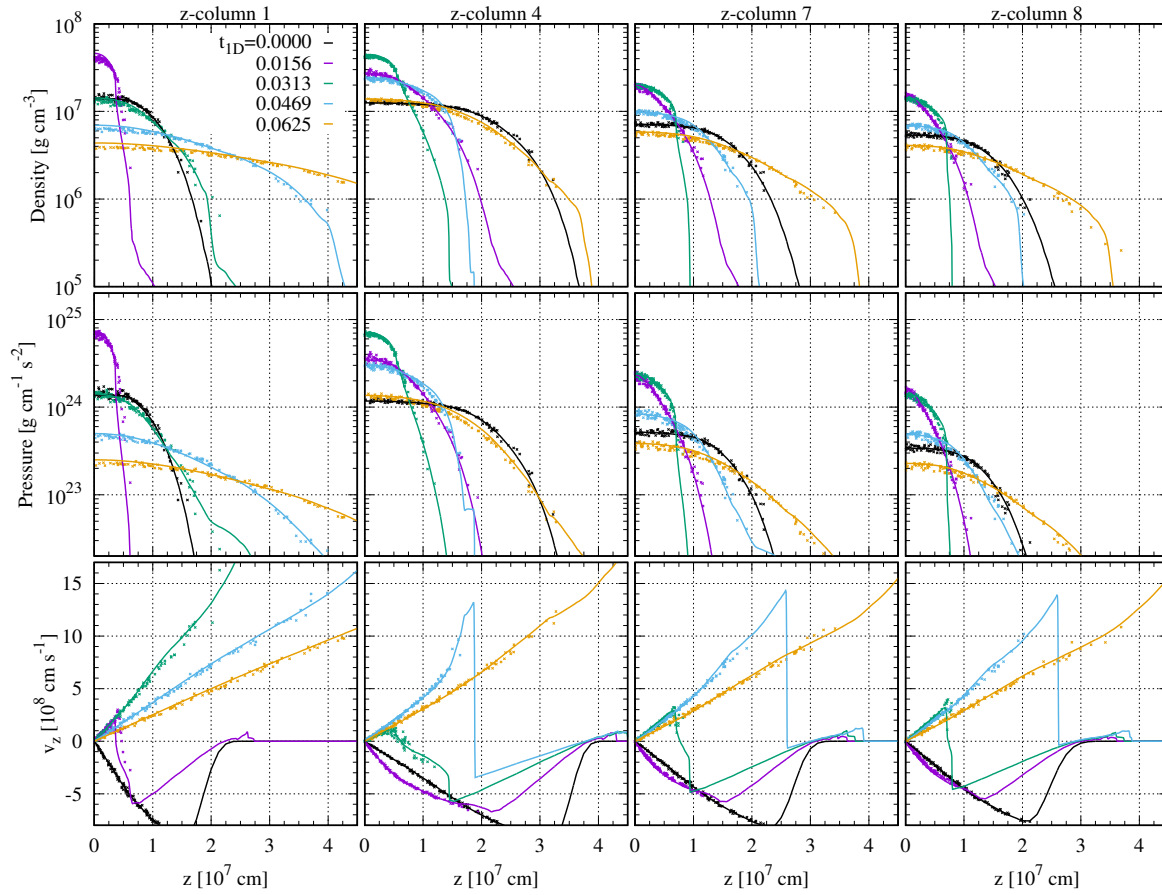


Figure A1. Density, pressure and z -velocity profiles in z -columns 1, 4, 7, and 8. Points indicate SPH particles sampled randomly from 3D SPH simulation for saving storage size. The number of the sampled particles for each z -column is about 300th of the number of all the particles in each z -column. Solid curves show the results of the 1D mesh simulation. For this comparison, we turn off nuclear reaction networks in the 1D mesh simulation.

A.2. Comparison between simulations with and without IMBH gravity

We perform 1D mesh simulations, including the IMBH gravity in the z -direction. We set separation between the z -columns and IMBH to 1.45×10^9 cm (see Figures 1 and 2). Figure A2 shows the z -velocity profiles just after pressure waves steepen into shock waves in the cases including the IMBH gravity. Tidal detonation occurs in z -columns 1 - 7, and does not in z -columns 8 - 9, which is the same as in the cases where we ignore the IMBH gravity. This is because pressure gradients in the z -columns are much larger than the IMBH gravity. For example, tidal detonation starts at $z \sim 10^7$ cm and $t_{1D} \sim 0.0352$ s in z -column 7 (see Figure 4). In that place, the pressure gradient and IMBH gravity are, respectively, $(\partial P / \partial z) / \rho \gtrsim 10^{10}$ cm s $^{-2}$ (see the curves of $t_{1D} = 0.0313$ s and 0.0469 s of z -column 7 panels in Figure A1) and $GM_{\text{IMBH}}z / R^3 \sim 10^8$ cm s $^{-2}$.

A.3. Modeling of the WD edge

As seen in the top panel of Figure 3, density structure in the 1D initial condition is extrapolated below 2×10^5 g cm $^{-3}$. This extrapolation does not affect the emergence of tidal detonation, since the tidal detonation emerges at a region reflecting information of 3D SPH simulation. In z -column 4, tidal detonation occurs where density is $> 10^6$ g cm $^{-3}$. On the other hand, materials in this z -column are compressed by a factor of at most 5 during its evolution. Therefore, the tidal detonation emerges at materials whose density is initially $> 2 \times 10^5$ g cm $^{-3}$. In other words, the tidal detonation occurs at a region reflecting 3D SPH simulation results.

As seen in the bottom panel of Figure 3, z -velocity structure in the 1D initial condition is slightly oversmoothed at the edge of the z -column. We investigate this oversmoothing on the emergence of tidal detonation. Using z -velocity structure in the 3D SPH simulation, we extrapolate z -velocity structure for z -column 4 in two different ways. One is that we set z -velocity to zero at $|z| = 4 \times 10^7$ cm discontinuously, and the other is that we increase the absolute value of z -velocity up to the boundary of the 1D mesh simulation (see the left panel of Figure A3). As seen in the second

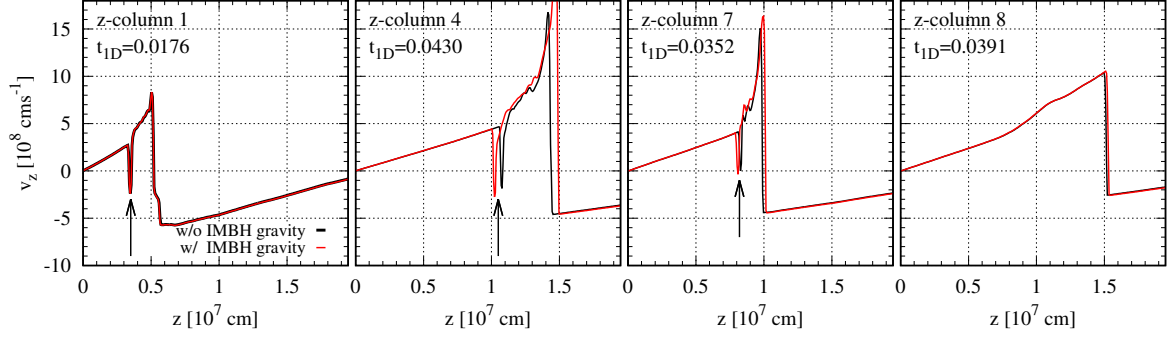


Figure A2. Profiles of z -velocity in z -columns 1, 4, 7, and 8 just after pressure waves steepen into shock waves. Red and black curves indicate with and without including the IMBH gravity in the z -direction, respectively. Arrows indicate reverse shock waves accompanying detonation waves.

and third left panels of Figure A3, the modeling of the WD edge affects the edge evolution of z -velocity (on the right side of the vertical dotted lines), however does not affect the internal evolution of z -velocity which raises pressure waves steepening into shock waves (on the left side of the vertical dotted lines). Finally, we can see in Figure A3 that tidal detonation emerges in both cases of the extrapolated 1D initial conditions, similarly to the original 1D initial conditions. Therefore, the oversmoothing z -velocity at the edge of z -columns does not affect the emergence of tidal detonation.

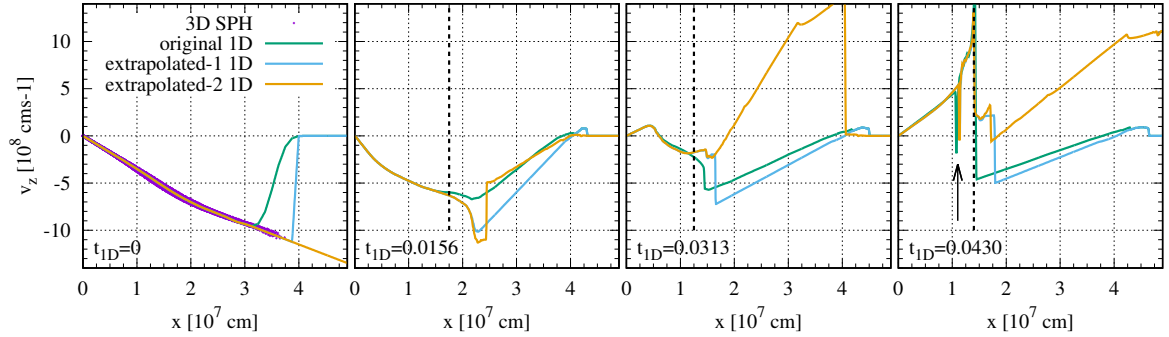


Figure A3. Time evolution of z -velocity profiles in z -column 4 for original and extrapolated 1D initial conditions. As a reference, we show the z -velocity profile in the 3D SPH simulation at $t_{\text{ID}} = 0$. The arrow indicates reverse shock waves accompanying detonation waves.

A.4. 1D resolution check

We perform a convergence check of 1D mesh simulations with different space resolution for z -columns 1, 4, 7, and 8. We change the mesh size from 6.25×10^4 cm to 0.78×10^4 cm. Note that the mesh size sufficiently resolves the hotspot size ($\sim 10^5$ cm). Figure A4 shows the time evolution of z -velocity profiles with different 1D space resolution. We find a good agreement among the results of different 1D space resolution. We conclude the results about the emergence of tidal detonation are converged among different 1D space resolution.

A.5. 3D resolution check

We perform a convergence check of 1D mesh simulations with different N_{sph} in 3D SPH simulations. Note that this is *not* a convergence check of space resolution in 1D mesh simulations. Figure A5 shows the time evolution of z -velocity profiles in z -columns 1, 4, 7, and 8 for 3D SPH simulations with $N_{\text{sph}} = 19\text{M}$, 75M , and 300M . We can see the presence of reverse shock waves in all N_{sph} cases for z -columns 1, 4 and 7. On the other hand, for z -column 8, a reverse shock wave is present in the $N_{\text{sph}} = 19\text{M}$ case, and absent in the the $N_{\text{sph}} = 75\text{M}$ and 300M cases. Eventually, we find tidal detonation succeeds in the $N_{\text{sph}} < 75\text{M}$ cases, and fails in the $N_{\text{sph}} \geq 75\text{M}$ cases for z -column 8.

In order to investigate the reason for the failure of tidal detonation in large- N_{sph} cases, we show density and z -velocity profiles in these z -columns just before shock waves appear in Figure A6. Just after this time, a pressure wave indicated by dashed lines will steepen into a shock wave immediately. Thus, the shock wave will heat the right-side region of the dashed line after this time. In all the z -columns, we can see density of the right-side region becomes

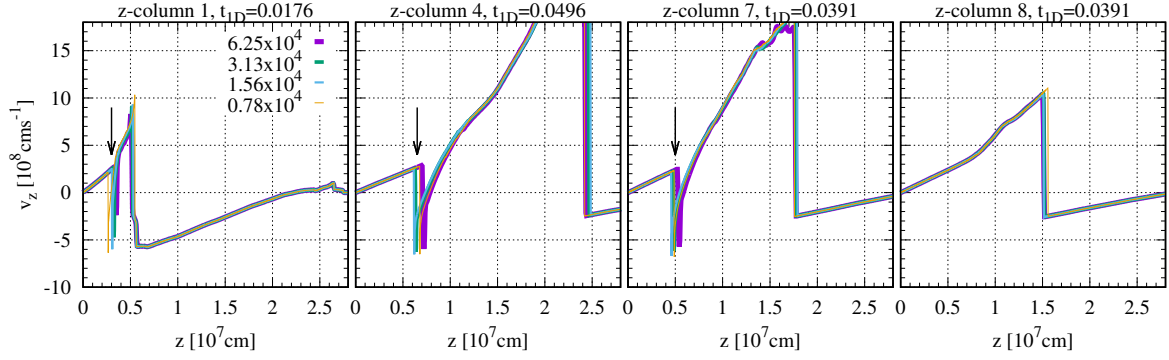


Figure A4. Profiles of z -velocity in z -columns 1, 4, 7, and 8 with different space resolution from 6.25×10^4 cm to 0.78×10^4 cm in 1D mesh simulations. The time is just after tidal detonation (or just a shock wave) appears. Arrows indicate reverse shock waves accompanying detonation waves.

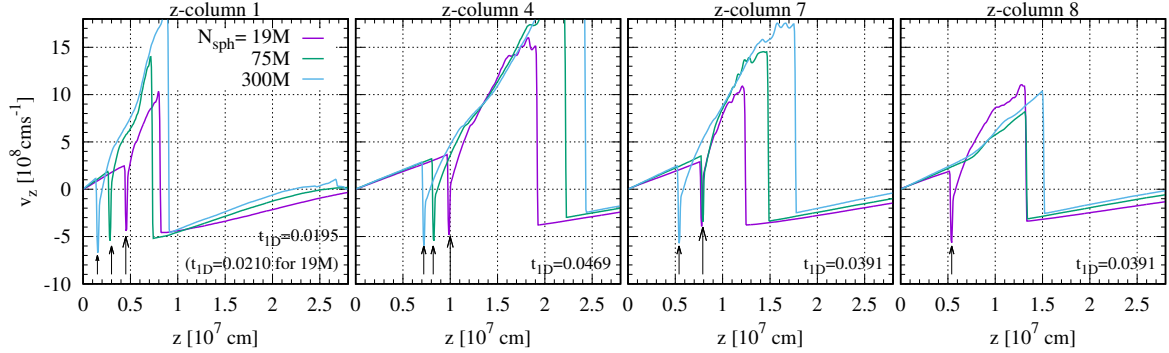


Figure A5. Profiles of z -velocity in z -columns 1, 4, 7, and 8 for 3D SPH simulations with the $N_{\text{sph}} = 19\text{M}$, 75M , and 300M cases. Arrows indicate reverse shock waves accompanying detonation waves.

smaller with N_{sph} increasing if $N_{\text{sph}} < 75\text{M}$. Since nuclear reactions proceed more rapidly with density higher, tidal detonation occurs more easily in smaller N_{sph} cases. In all the z -columns, density profiles in the $N_{\text{sph}} \geq 75\text{M}$ cases are the same. Therefore, the 1D mesh simulations are converged in the range from $N_{\text{sph}} = 75\text{M}$ to $N_{\text{sph}} = 300\text{M}$. In other words, tidal detonation fails in z -column 8, and tidal detonation will succeed in z -columns 1, 4 and 7 even if N_{sph} becomes infinite.

The reason for the unconvergence in the $N_{\text{sph}} < 75\text{M}$ cases is that initial conditions of 1D mesh simulations in the $N_{\text{sph}} < 75\text{M}$ cases are not converged, since the results of 3D SPH simulations are not converged especially at the WD edge. Figure A7 shows the initial conditions of z -column 8 in 3D SPH simulations with $N_{\text{sph}} = 4.7\text{M}$ to 300M . At the edge of the z -column, density decreases with N_{sph} increasing. Generally, SPH methods can capture edge structure sharply with N_{sph} increasing, since SPH kernel length becomes smaller with N_{sph} increasing. Therefore, density at the edge is overestimated, and tidal detonation occurs falsely for smaller- N_{sph} cases.

REFERENCES

- Auchettl, K., Guillochon, J., & Ramirez-Ruiz, E. 2017, *ApJ*, 838, 149
- Balsara, D. S. 1995, *Journal of Computational Physics*, 121, 357
- Brassart, M., & Luminet, J.-P. 2008, *A&A*, 481, 259
- Cheng, R. M., & Bogdanović, T. 2014, *PhRvD*, 90, 064020
- Clausen, D., & Eracleous, M. 2011, *ApJ*, 726, 34
- Colella, P., & Woodward, P. R. 1984, *Journal of Computational Physics*, 54, 174
- Dehnen, W., & Aly, H. 2012, *MNRAS*, 425, 1068
- East, W. E. 2014, *ApJ*, 795, 135
- Fryxell, B., Olson, K., Ricker, P., et al. 2000, *ApJS*, 131, 273
- . 2010, FLASH: Adaptive Mesh Hydrodynamics Code for Modeling Astrophysical Thermonuclear Flashes, *Astrophysics Source Code Library*, ascl:1010.082
- Haas, R., Shcherbakov, R. V., Bode, T., & Laguna, P. 2012, *ApJ*, 749, 117
- Holcomb, C., Guillochon, J., De Colle, F., & Ramirez-Ruiz, E. 2013, *ApJ*, 771, 14
- Ioka, K., Hotokezaka, K., & Piran, T. 2016, *ApJ*, 833, 110
- Iwasawa, M., Tanikawa, A., Hosono, N., et al. 2016, *PASJ*, 68, 54
- Kawana, K., Tanikawa, A., & Yoshida, N. 2017, *ArXiv e-prints*, arXiv:1705.05526
- Kobayashi, S., Laguna, P., Phinney, E. S., & Mészáros, P. 2004, *ApJ*, 615, 855
- Komossa, S. 2015, *Journal of High Energy Astrophysics*, 7, 148
- Krolik, J. H., & Piran, T. 2011, *ApJ*, 743, 134
- . 2012, *ApJ*, 749, 92

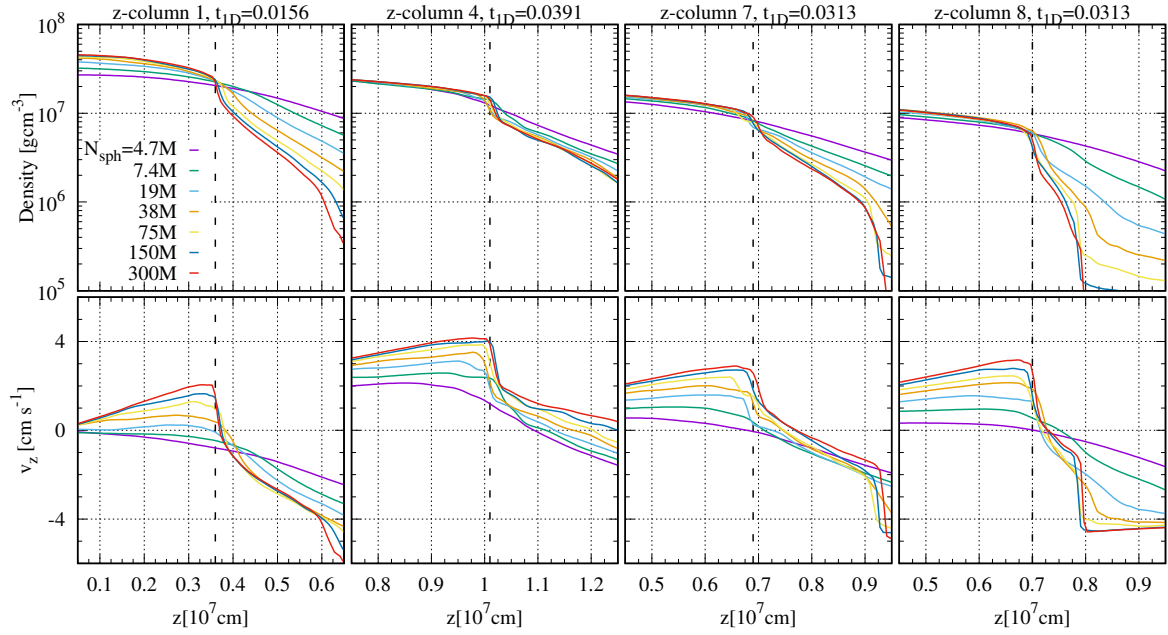


Figure A6. Density and z -velocity profiles in z -columns 1, 4, 7, and 8 just before shock waves appears. The 3D SPH resolution is $N_{\text{sph}} = 4.7\text{M}$, 9.4M , 19M , 38M , 75M , 150M , and 300M . Dashed lines indicate the position of a pressure wave to be a shock wave immediately.

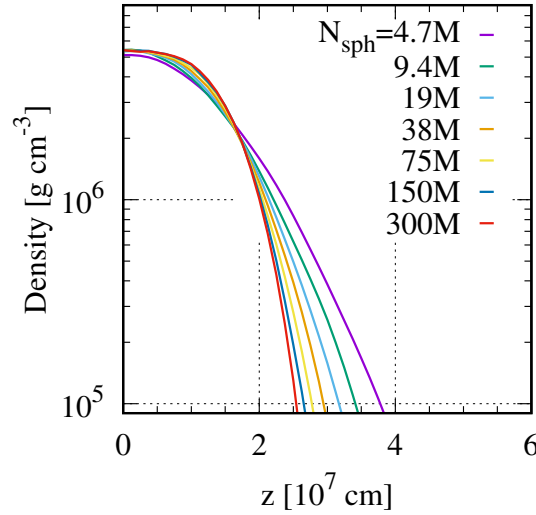


Figure A7. Density profile in z -column 8 at the initial time, based on 3D SPH simulation with different N_{sph} .

Law-Smith, J., MacLeod, M., Guillochon, J., Macias, P., & Ramirez-Ruiz, E. 2017, *ApJ*, 841, 132
Luminet, J.-P., & Pichon, B. 1989, *A&A*, 209, 103
MacLeod, M., Goldstein, J., Ramirez-Ruiz, E., Guillochon, J., & Samsing, J. 2014, *ApJ*, 794, 9
MacLeod, M., Guillochon, J., Ramirez-Ruiz, E., Kasen, D., & Rosswog, S. 2016, *ApJ*, 819, 3
Monaghan, J. J. 1997, *Journal of Computational Physics*, 136, 298
Morris, J. P., & Monaghan, J. J. 1997, *Journal of Computational Physics*, 136, 41
Parsons, S. G., Gänsicke, B. T., Marsh, T. R., et al. 2017, *MNRAS*, 470, 4473
Price, D. J., & Monaghan, J. J. 2007, *MNRAS*, 374, 1347
Rosswog, S., Ramirez-Ruiz, E., & Hix, W. R. 2009, *ApJ*, 695, 404

Rosswog, S., Ramirez-Ruiz, E., Hix, W. R., & Dan, M. 2008, *Computer Physics Communications*, 179, 184
Shiokawa, H., Krolik, J. H., Cheng, R. M., Piran, T., & Noble, S. C. 2015, *ApJ*, 804, 85
Stone, N., Sari, R., & Loeb, A. 2013, *MNRAS*, 435, 1809
Stone, N. C., Kesden, M., Cheng, R. M., & van Velzen, S. 2018, *ArXiv e-prints*, arXiv:1801.10180
Tanikawa, A., Nakasato, N., Sato, Y., et al. 2015, *ApJ*, 807, 40
Tanikawa, A., Sato, Y., Nomoto, K., et al. 2017, *ApJ*, 839, 81
Tanikawa, A., Yoshikawa, K., Nitadori, K., & Okamoto, T. 2013, *NewA*, 19, 74
Tanikawa, A., Yoshikawa, K., Okamoto, T., & Nitadori, K. 2012, *NewA*, 17, 82
Tchekhovskoy, A., Metzger, B. D., Giannios, D., & Kelley, L. Z. 2014, *MNRAS*, 437, 2744

- Tejeda, E., & Rosswog, S. 2013, MNRAS, 433, 1930
- Timmes, F. X., & Swesty, F. D. 2000, ApJS, 126, 501
- van Velzen, S., Frail, D. A., Körding, E., & Falcke, H. 2013, A&A, 552, A5
- van Velzen, S., Körding, E., & Falcke, H. 2011, MNRAS, 417, L51
- Wendland, H. 1995, Advances in Computational Mathematics, 4, 389
- Wilson, J. R., & Mathews, G. J. 2004, ApJ, 610, 368
- Zalamea, I., Menou, K., & Beloborodov, A. M. 2010, MNRAS, 409, L25